ACS APPLIED MATERIALS & INTERFACES

www.acsami.org

Research Article

Tiled Monolayer Films of 2D Molybdenum Disulfide Nanoflakes Assembled at Liquid/Liquid Interfaces

Joseph Neilson, Michael P. Avery, and Brian Derby*

Cite This: *ACS Appl. Mater. Interfaces* 2020, 12, 25125–25134

Read Online

ACCESS | Metrics & More | Article Recommendations | Supporting Information

ABSTRACT: Thin films of MoS_2 bilayer nanoflakes, which are predominantly a single flake thick and with flakes in edge-to-edge contact, have been produced via self-assembled tiling at the planar interface between two immiscible liquids. Films of several square centimeters extent can be produced with a total covered area approaching 90% and over 70% of the film covered by single flakes without overlap. Films produced through liquid/liquid assembly are shown to produce a lower uncovered area fraction and more uniform thickness when compared with films of similar areal coverage produced by the "top-down" techniques of spin coating and spray coating. Statistical analysis of flake coverage data, measured by atomic force microscopy (AFM), shows that liquid/liquid assembly produces a distinctly different variation in film thickness than conventional top-down deposition. This supports the hypothesis that the two-dimensional (2D) confinement of liquid/liquid assembly produces more uniform films. Demonstrator field-effect transistors (FETs) manufactured from the films exhibit mobility and on/off current ratios of 0.73 $cm^2\ V^{-1}\ s^{-1}$ and 10^5, respectively, comparable to FETs of similar layout and chemical vapor deposition (CVD)-grown or mechanically cleaved single-crystal MoS_2 channel material. This work demonstrates the use of liquid/liquid interfaces as a useful tool for the self-assembly of high-performance thin-film devices made from dispersions of 2D materials.

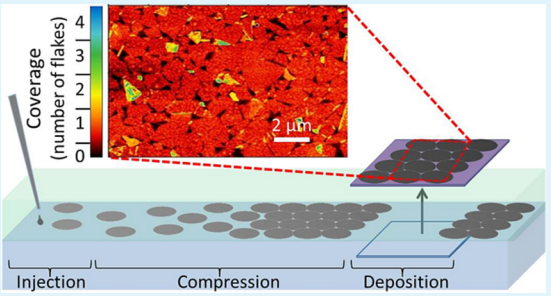

KEYWORDS: *thin films, 2D materials, Poisson distribution, coverage, self-assembly, device fabrication*

INTRODUCTION

Semiconducting transition metal dichalcogenides (TMDC), such as molybdenum disulfide (MoS_2), have a layered crystal structure analogous to graphene, with the layers bonded by relatively weak van der Waals bonds, and can be exfoliated to form thin flakes of two-dimensional (2D) materials.[1] These materials have unique physical properties that are tunable, depending on the number of atomic layers in the flakes, and have been widely explored for use in the fabrication of electronic and optoelectronic devices such as field-effect transistors (FETs) and optical sensors.[2−4]

Large-area crystalline MoS_2 films can be grown using "bottom-up" methods such as chemical vapor deposition (CVD), leading to high-quality electronic and optoelectronic devices.[5,6] However, the high-temperature requirement of the CVD process does not allow the direct deposition of large-area devices onto flexible polymeric substrates. At present, the leading technology for low-cost, large-area flexible electronics manufacture is organic semiconductor technology, which is compatible with a range of relatively low-cost printing methods and roll-to-roll manufacturing. However, current generation organic FETs suffer from relatively low carrier mobility compared to inorganic semiconductor devices, which limits their applications.[7] In contrast, devices produced from liquid dispersions (inks) of TMDCs have potentially higher carrier mobility and could therefore represent an attractive, printable alternative to organic semiconductors with superior performance, while allowing new flexible device types to be produced. To make printed large-area thin films from 2D TMDCs for high-throughput manufacture of electronic devices, solution-based processing provides a low-cost and low-temperature option. The exfoliation and handling of 2D materials as colloids is already widely explored[8] and has enabled the formulation of printable inks for use in flexible electronic devices that have the potential to be mass produced, e.g., by roll-to-roll manufacturing.[9]

The fabrication of large-area films from a colloidal dispersion of nanosheets is a key challenge for the manufacture of electronic devices from solution-processed 2D materials. A number of solution-based methods have been developed to produce thin films of 2D materials; these can be grouped into: (1) "top-down" methods, e.g., spray coating[10] and spin coating,[11] where flakes are deposited from the surrounding

Received: February 27, 2020
Accepted: May 8, 2020
Published: May 8, 2020

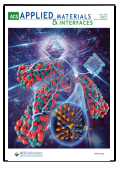

https://dx.doi.org/10.1021/acsami.0c03794
ACS Appl. Mater. Interfaces 2020, 12, 25125−25134

medium and fall randomly onto the final substrate, remaining attached at their initial contact position; and (2) "interface assembly" methods at liquid/air (Langmuir–Blodgett)[12−14] or liquid/liquid interfaces,[15−21] where flakes are confined to the interface between two phases and assemble through translation within the interface, before transfer of the complete resulting film onto a substrate. Although the Langmuir–Blodgett method for assembly at the liquid/air interface is well established, material can be lost to mixing with the subphase and aggregation can occur during assembly.[18] In addition, the large subphase area is sometimes unsuitable for research scale film assembly.[22] These issues can be ameliorated by assembly at liquid/liquid interfaces, which have been shown to improve confinement of material to the interface without the need for specialized apparatus and can be applied to a range of 2D, 1D, and 0D materials.[14,15,18,23]

Carrier mobility is higher in-plane than out-of-plane for 2D materials, due to the tunnel barrier through the van der Waals gap; thus edge-to-edge contacts between nanoflakes and dense packing within the plane are beneficial to ensure high carrier mobility throughout a 2D material film.[24−27] Improved edge-to-edge contact and reduced overlap can be afforded by interfacial assembly methods, which confine material at the molecularly flat interface, therefore offering a more promising route to high-quality thin films than top-down assembly methods.

The assembly of 2D materials at planar liquid/liquid interfaces can be achieved in a number of ways. Most literature examples report methods that begin by dispersing the 2D material in one liquid, before adding a second immiscible liquid layer to create the interface. The 2D material in the dispersed phase can be induced to transport to the interface using mechanical means, such as sonication or manual shaking,[16,20,21] or by the addition of a chemical inducing agent.[19,28] There have been few reports of assembly by direct injection of the material to the liquid/liquid interface, as described in this work.[17,18]

Here, we demonstrate the assembly of predominantly bilayer flakes of MoS_2 at the interface between two immiscible solvents (hexane and water). Water and hexane were selected to form the interface for film assembly due to their high interfacial tension of around 50.5 mN m^{-1},[29] which can be effectively lowered by the insertion of a monolayer of 2D material, promoting liquid/liquid interfacial assembly. Isopropyl alcohol (IPA) was selected as the solvent for dispersing MoS_2, due to its well-matched solubility parameters, low toxicity, and miscibility with both water and hexane.[30] The morphology of the resulting films is compared with those produced by spray coating and spin coating. The films fabricated at liquid/liquid interfaces are shown to have greater film uniformity and single-layer coverage than found with the top-down deposited films.

RESULTS AND DISCUSSION

MoS_2 Nanoflake Dispersion. A dispersion of MoS_2 nanoflakes in isopropyl alcohol (IPA) was obtained as described in the Materials and Methods section. The dispersion contained flakes of average area 0.95 μm^2 and thickness 2 nm as determined by scanning electron microscopy (SEM) and atomic force microscopy (AFM), respectively (Figure 1a,b) (histogram of flake lateral area data is in the Supporting Information, Figure S1). The semiconducting 2H phase of MoS_2 is retained as evidenced by the a, b, and c

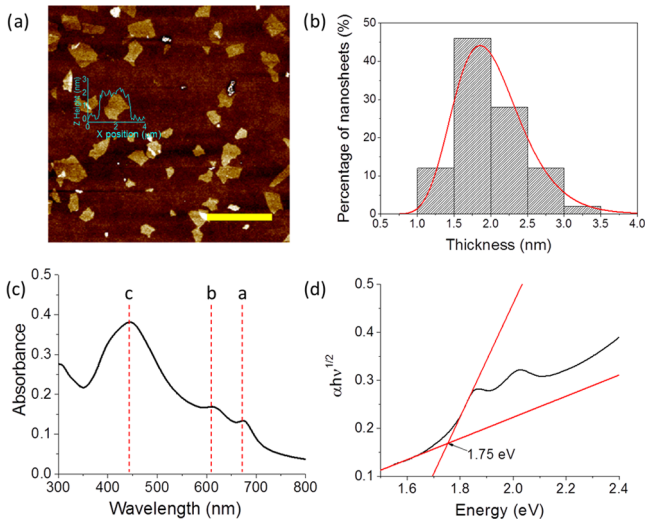

Figure 1. (a) AFM image of MoS_2 flakes produced from cascade centrifugation fraction 8−12 kRPM, spin-coated onto a Si/SiO_2 wafer (scale bar = 5 μm). (b) Histogram of nanoflake height distribution from AFM data (n = 50). (c) Absorbance spectra for MoS_2 dispersion in IPA (10× dilution); excitonic peaks a, b, and c are indicated. (d) Tauc plot for the MoS_2 dispersion using the indirect allowed transition model.

excitonic peaks at around 673, 610, and 445 nm, respectively (Figure 1c). The a and b peaks correspond to the σ−d interband electronic transitions associated with the d2 metal in the hexagonal coordination geometry.[31] The c excitonic peak is also typical of 2H phase MoS_2 absorption spectra and has been linked to a Van Hove singularity.[32] The Tauc plot in Figure 1d suggests a band gap energy of around 1.75 eV, indicative of one- to two-layer MoS_2.[33,34]

Stability of Nanoflakes at the Liquid/Liquid Interface. The adsorption of a solid particle at a fluid–fluid interface is driven by the reduction of the interfacial energy of the system.[15,16,35−38] The energy of detachment of the particle into either liquid 1 or liquid 2, E_{d1} and E_{d2}, is given by[36]

$$E_{d1} = \gamma_{12}(A_c + A_{p2}\cos\theta) \quad (1a)$$

$$E_{d2} = \gamma_{12}(A_c - A_{p1}\cos\theta) \quad (1b)$$

Here, γ_{12} is the interfacial tension between the two liquids, A_c is the change in the liquid 1/liquid 2 interfacial area resulting from the detachment of the particle, θ is the three-phase contact angle, and A_{p1}, A_{p2} are the initial areas of the particle/liquid interface prior to the detachment of the particle for liquids 1 and 2, respectively. The lowest energy of detachment E_d is given by

$$E_d = \begin{cases} E_{d2} & \text{for } 0° \le \theta \le 90° \\ E_{d1} & \text{for } 90° \le \theta \le 180° \end{cases} \quad (2)$$

For all values of θ, the detachment energy is positive, with a maximum value at θ = 90°. It is therefore thermodynamically favorable for particles to gather at the interface, and they do so spontaneously.[36] The energy required to detach particles from the interface can be several orders of magnitude greater than k_BT, under the correct conditions, making these very stable systems.[15,35−39] The detachment energy increases with increasing particle size since the A_c, A_{p1}, and A_{p2} terms all increase, provided that particles remain small enough (typically

https://dx.doi.org/10.1021/acsami.0c03794
ACS Appl. Mater. Interfaces 2020, 12, 25125−25134

a few microns in diameter, d, for spherical particles) that the effects of gravity are negligible.[38,39] This is confirmed by the Bond number ≪1 (Supporting Information, eq S1) for particles of diameter 1 μm.

When discussing the behavior of particles at liquid/liquid interfaces, the typical model system, applicable to most colloidal particle behavior, is that of a spherical particle (radius, r) at a flat horizontal interface. For spherical particles, eq 2 becomes

$$E_d = \pi r^2 \gamma_{hw}(1 \pm \cos\theta)^2 \tag{3}$$

Here, the sign in the parentheses is positive when $\theta > 90°$ and negative when $\theta < 90°$.[36,38] Note that we have replaced the subscripts 1 and 2 with h and w to represent hexane and water, respectively, which are the solvents used in this study.

Spherical particles are, however, not an appropriate description for 2D flake materials. Equation 2 can also be used to describe systems of nonspherical particles, such as rods or disks. Binks provides an analysis for a rounded disklike particle based on the major (a) and minor (b) semiaxes of the particle such that a/b is the particle aspect ratio.[36]

$$E_{dw} = \pi b^2 \gamma_{hw}(1 - \cos\theta)^2 \left[1 + \frac{\left(\frac{a}{b} - 1\right)^2}{1 - \cos\theta} + \frac{2\left(\frac{a}{b} - 1\right)(\sin\theta - \theta\cos\theta)}{(1 - \cos\theta)^2}\right] \tag{4a}$$

$$E_{dh} = E_{dw} + 2\pi b^2 \gamma_{hw} \cos\theta \left[\left(\frac{a}{b} - 1\right)^2 + \pi\left(\frac{a}{b} - 1\right) + 2\right] \tag{4b}$$

Although flakes of 2D materials at liquid/liquid interfaces have been described by this rounded disk model previously,[16] we suggest a simpler approximation to the flake geometry. We treat the flakes as infinitesimally thin disks where the disk edge has a negligible contribution to the flake area when compared to the faces of the disk. The most stable configuration of the flake at the interface, where E_d is maximized and the interfacial energy is minimized, is with the flake faces parallel to the interface, maximizing A_c. For this system, $A_c = A_{pw} = A_{ph} = A_f$, where A_f is the area of one face of the disk. The minimum energy for detachment for 2D flakes given by eq 2 therefore simplifies to

$$E_d = \gamma_{hw} A_f (1 \pm \cos\theta) \tag{5}$$

where the sign in the parentheses is positive when $\theta > 90°$ and negative when $\theta < 90°$.

Applying eq 5 to our experimental system, γ_{hw} = 50.5 mJ m^{-2}, A_f = 0.95 μm^2 (Supporting Information, Figure S1), and θ = 99.7° (determined by the sessile drop method (Supporting Information, Figure S4)), we find that E_d is 9.70 × 10^6 k_BT. This value is almost identical to the value calculated using eqs 4a and 4b for the rounded disk model (a = 0.55 μm, b = 1 nm), validating our simplified approach for 2D materials at liquid/liquid interfaces and confirming that the contribution of flake edges to the reduction in interfacial energy at the interface is indeed negligible. By comparison, E_d for a spherical particle of equal total surface area is 6.19 × 10^5 k_BT, as calculated using eq 3. Thus, the stability of confinement at the liquid/liquid interface is greater for disklike particles and flakes of 2D materials than for spherical particles, further increasing the driving force for assembly.

Liquid/Liquid Film Assembly. Figure 2b provides a schematic illustration of the three-step process for film assembly and transfer onto a substrate. The dispersed 2D material is injected into the upper hexane phase, and the flakes assemble at the liquid/liquid interface driven by the reduction in interfacial energy, as discussed above. The high energy required to detach flakes from the interface, as described by eq 5, ensures minimal overlap between adjacent flakes during the assembly process. The IPA used to disperse the flakes causes a decrease in the water/hexane interfacial tension at the point of injection;[40] hence, the resulting local interfacial tension gradient sweeps the 2D material to the opposite side of the interface. This effect is evident at the macroscopic scale, as shown in Figure 2a (see also Video S1 in the Supporting Information). The interfacial tension gradient compresses the individual nanoflakes into a tightly packed, tiled film, with enhanced edge-to-edge contact and connectivity of the flakes within the thin film (high-magnification SEM image available in the Supporting Information, Figure S2). The assembled film of densely tiled (jammed) 2D flakes is stable at the liquid/liquid interface for at least 2 days, with no mixing of the 2D material with either bulk phase observed. This can be attributed to the poor solubility of MoS_2 materials in both hexane and water, and its stability at the interface of hexane and water. Finally, the film is transferred onto a substrate by manually lifting it through the film parallel to the interface, analogous to the Langmuir−Schaeffer coating method (Figure 2b).[41,42]

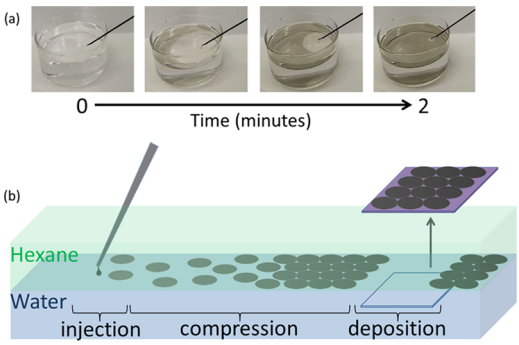

Figure 2. (a) Large-scale assembly (interface diameter = 8 cm) of 2D nanoflake material at the water/hexane interface by injection of IPA dispersion from 0 to 2 min. Video of this assembly process is given in the Supporting Information, Video S1. (b) Schematic representation of the steps involved in the film assembly: (1) Material is injected at the interface of hexane and water, (2) the surface tension gradient acts to compress the flakes into a maximally jammed 2D film, and (3) the substrate is lifted through the assembled interface film, and the thin film is deposited.

Hence, this liquid/liquid film assembly method is applicable to many 2D materials, and a variety of substrates can be coated in this way. Additional benefits of the injection method discussed here over previously reported liquid/liquid methods are improved control over the amount of material added to the interface and a reduced number of processing steps without the need for further sonication or an inducing agent to facilitate film formation.

https://dx.doi.org/10.1021/acsami.0c03794
ACS Appl. Mater. Interfaces 2020, 12, 25125−25134

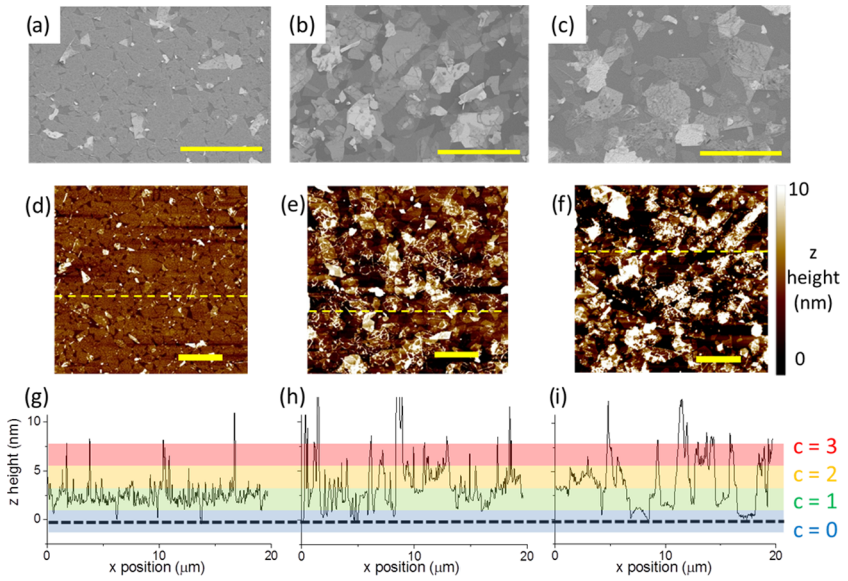

Figure 3. SEM images of MoS_2 thin films using: (a) liquid/liquid interface assembly; (b) spin coating; and (c) spray coating. AFM images of MoS_2 thin films deposited using: (d) liquid/liquid interface assembly, (e) spin coating, and (f) spray coating. (g–i) Line scans from the AFM images (d–f) corresponding to the dashed yellow lines. The colored regions indicate the z height in terms of coverage (c) in flake monolayers. The black dotted line corresponds to the height of the substrate. All scale bars = 5 μm.

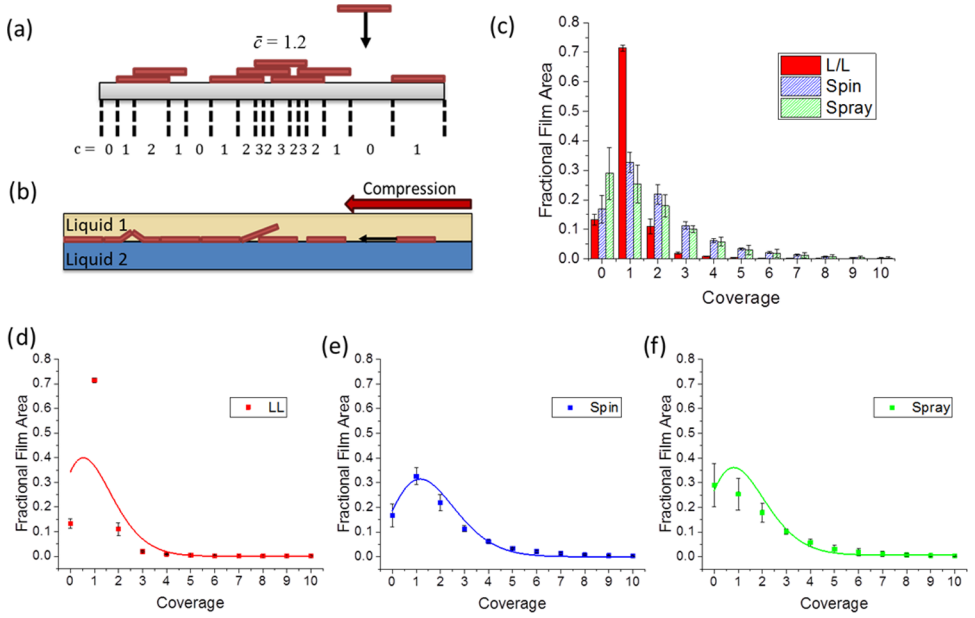

Figure 4. (a) Schematic vertical slice through a substrate on which objects of identical dimensions have been deposited providing a visualization of coverage (c) and mean coverage ($\bar{c}$). (b) Vertical slice through the liquid/liquid interface providing a visualization of film formation at the interface. (c) Histogram of flake coverage for liquid/liquid (LL), spin-coated (spin), and spray-coated (spray) films. Data is the average of four scanned areas (20×20 μm^2) at different locations on each film. Individual plots of fractional film area versus coverage for: (d) liquid/liquid, (e) spin-coated, and (f) spray-coated films; solid lines are the result of fitting to a Poisson distribution with statistical weighting.

Characterization of Films on Substrates. Figure 3 shows representative SEM and AFM images of MoS_2 films on a Si wafer (90 nm SiO_2) formed via liquid/liquid interfacial assembly, spin coating, and spray coating with similar mean coverage. Films formed by spray and spin coating contain stacked/overlapped flakes and a large fraction of uncovered area. The liquid/liquid interface assembly method, however, confines flakes to a single assembly plane. This leads to minimal flake/flake overlap and clear edge-to-edge contact between the majority of the flakes (Figure 3a,d) (high-magnification SEM image available in the Supporting Information, Figure S2); the resulting film is therefore continuous and well packed, with an average coverage of 89% (AFM, Figure 3a) to 91% (SEM, Figure 3b), similar to the predicted packing fraction for maximally jammed binary hard disks (0.78–0.91).[43−48] The z-height data in the AFM images can also be extracted and processed to provide a quantitative measure of the distribution of flakes on the substrate via the assignment of coverage values.

Coverage is a dimensionless discrete variable, c, giving the number of objects that intersect a line perpendicular to a surface at a given point. The mean coverage, $\bar{c}$, is given by the

https://dx.doi.org/10.1021/acsami.0c03794
ACS Appl. Mater. Interfaces 2020, 12, 25125−25134

number of objects per unit area multiplied by the area of one object.[49,50] A visual representation of these concepts is given in Figure 4a. For top-down deposition, such as spin coating and spray coating, the arrival of material at the surface can be treated as a series of independent random events, and thus, given the finite size of the flakes, overlap of the arriving material is possible. In this case, the probability, $P(c|\bar{c})$, that a point on the surface has a coverage, c, when the whole surface has a mean coverage $\bar{c}$, is given by the Poisson distribution[49,50]

$$P(c \mid \bar{c}) = \frac{e^{-\bar{c}}\bar{c}^{c}}{c!} \text{ for } c = 0, 1, 2, 3, \ldots \quad (6)$$

When film assembly occurs at an interface, if the concentration of the flake dispersion is sufficiently dilute, there will be minimal overlap and face-to-face contact of the flakes with each confined to the 2D interface on injection. The flakes at the interface are then compressed into a tightly packed film via an interfacial tension gradient, resulting from the material injection,[40] as previously discussed. We also note that capillary/electrostatic forces may also compress the film over a short range, but such effects are expected to be slight for particles of thickness <100 nm.[51,52] If compression forces are large enough, this may lead to localized film buckling or overlap such as that shown in Figure 4b, despite the 2D constraint of the interface. Further compression and roughening of the film may also occur as part of the assembled film transfer process. The expected final mean coverage for 2D films assembled at interfaces in this case is, thus, $\bar{c} \approx 1$. If the flakes were truly confined to the interface, forbidding overlap from occurring, then we would expect $\bar{c} < 1$ because perfect tiling of irregular flakes is not possible.

Thus, from our consideration of the mechanisms leading to the formation of a film through the addition of individual 2D material flakes, we would expect that the top-down deposition methods will show a range of film thicknesses over a given area, described by the Poisson distribution. In contrast, films produced by interfacial assembly should show a more singular distribution of thicknesses dominated by a thickness defined by the expected dimensions of a single flake.

The histogram of AFM data given in Figure 4c, for the films produced by liquid/liquid assembly, spin coating, and spray coating, provides an experimental measure of the film coverage probability distribution. This shows the fractional areas of the resulting films with coverages 0, 1, 2, etc. (analysis of AFM data for four 20 × 20 μm^2 areas at different locations on each film). The bins for the histogram data were chosen based on average flake height measurements (Figure 1b), which found that MoS_2 flakes had an average height of 2 nm, with a minimum flake height of 1 nm. The height of a point on a film surface can be roughly equated to the coverage at that point by dividing by the height of a single flake. Therefore, any pixels in AFM film scans with a measured height <0.94 nm were treated as uncovered ($c = 0$), and increasing coverages were binned with bin widths of 2 nm from that value to correspond to an additional flake layer, i.e., 1−3 nm is $c = 1$, 3−5 nm is $c = 2$, and so on. It should be noted that this method introduces some error by miscounting the coverage for overhangs and subsurface holes in the film, but such miscounts should be relatively small in number.

From Figure 4c, the film produced using the liquid/liquid interface indeed shows the expected almost singular distribution of film thicknesses. The total covered area is 0.87 (1 minus area of zero coverage) with the majority of that area only covered by a single layer of flakes (0.71). This is further evidenced by the X-ray diffraction (XRD) pattern for the liquid/liquid assembled film that displays no 002 peak, which suggests that minimal stacking has occurred (Supporting Information, Figure S5).[53,54] The measured value for the total covered area is close to that found from the analysis of SEM images (0.89) and agrees well with theoretical packing fractions for maximally jammed systems of hard disks in 2D planes (0.78−0.906).[43−48] Nonzero values for coverages of 2 and greater show evidence that some flake overlap occurs, possibly due to the compressive mechanisms suggested earlier. By comparison, the coverage distributions for the top-down methods (spray and spin coating) are much broader with a greater proportion of the film area exhibiting coverages of 2 or more and an increased proportion of uncovered area ($c = 0$).

To test if the coverage distributions for the top-down methods describe a stochastic flake deposition process, as we would expect, they must be compared to a Poisson distribution. Figure 4d−f shows separate plots of the coverage histograms for the liquid/liquid, spin, and spray-coated films, given in Figure 4c, respectively. Each data set is fitted to a Poisson distribution for the appropriate mean coverage, shown by a solid line. The fit to a Poisson distribution is good for spin-coated and reasonably good for sprayed films ($R_{adj}^2 = 0.92$ and 0.85, respectively). This validates our description of these processes as a series of random flake deposition events at the interface. As expected, the fit is poor for the liquid/liquid assembled film ($R_{adj}^2 = 0.23$) clearly differentiating the film production mechanism used in this case.

Thin-Film Transistors. Thin-film transistors were manufactured using the liquid/liquid interface assembled MoS_2 film as the channel material. The devices demonstrate good repeatability (device repeatability test data is available in the Supporting Information, Figure S3). The electronic performance of an example FET is shown in Figure 5c,d, with peak mobility $\mu = 0.73$ cm^2 V^{-1} s^{-1} and on/off ratio = 10^5. This is comparable to previously reported CVD-grown FETs and FETs assembled using pristine mechanically cleaved few-layer MoS_2 single crystals with a back gate geometry and SiO_2 as the gate dielectric.[55,56] The devices also demonstrate superior properties to most solution-processed MoS_2 FETs reported in the literature (Figure 6).

However, the mobility value for our device is reduced in comparison to previously reported work using the same MoS_2 flake preparation method and a spin-coating film preparation method.[57] This discrepancy is likely due to a number of factors. We expect that around an order of magnitude mobility enhancement may be achievable by reducing coulomb scattering effects via the addition of a high-κ dielectric coating,[56−58] and further enhancement may be achievable by sulfur vacancy passivation via TFSI superacid surface treatment.[52,59] We also note that our device testing was conducted under ambient conditions, and around a 4-fold improvement to mobility can be expected by testing under vacuum as in the previous report.[60]

We ascribe the relatively high device performance of these simple FETs to: decreased contact resistance of the edge-to-edge contacts between flakes in the film,[25] minimal heterojunction barriers due to narrow nanoflake thickness distribution and minimal stacking,[61] and increased gate field modulation resulting from the ultrathin and flat nature of the film produced via liquid/liquid interface assembly. As we have shown, such high-quality films are easily produced via this

https://dx.doi.org/10.1021/acsami.0c03794
ACS Appl. Mater. Interfaces 2020, 12, 25125−25134

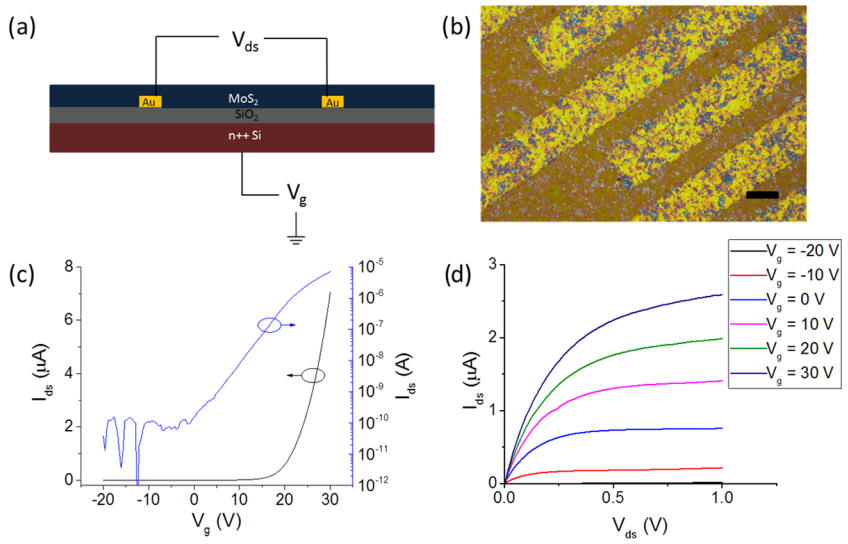

Figure 5. (a) Device layout for the prepared FETs. (b) Optical microscopy image of the thin film coating the source/drain electrodes of an assembled FET. Scale bar = 20 μm. (c) Transfer and (d) output curves for an assembled FET with a channel length of 10 μm. V_{ds} = 0.5 V for the transfer curve.

method, with minimal parameter optimization, resulting in films with less flake overlap than conventional spin-coating or spray-coating methods. Therefore, by combining the benefits of liquid/liquid interface assembly of thin films with the optimization of device performance via the methods outlined above, vastly improved device characteristics could be achieved in future studies.

CONCLUSIONS

Densely packed and predominantly single-layer films of flakes of 2D MoS_2 have been produced via assembly at the interface between two immiscible liquids, driven by gradients in interfacial tension. This is shown to be consistent with simple models for particle assembly at the liquid/liquid interface, which have been adapted for 2D material systems with negligible thickness. On comparison with films made using spray- or spin-coating deposition methods, the liquid/liquid assembled films show greater packing density (reduced uncovered area), an increased proportion of edge-to-edge contacts (reduced flake overlap), a greater area covered by a single-flake thickness (c = 1), and thus a reduced film roughness (a narrow distribution of coverages). The films have 13% uncovered area, consistent with random tiling models, and are on average 2 nm thick.

Statistical analysis of coverage data, measured using AFM, for films produced by liquid/liquid assembly and two other common, top-down film assembly methods, spin coating and spray coating, highlighted the differences in the deposition mechanisms. The distribution of flake coverage for top-down methods is well described by a Poisson distribution suggesting the stochastic nature of flake placement, whereas the liquid/liquid method shows a more singular distribution of coverages, indicative of flake confinement at the liquid/liquid interface.

Transistors were assembled using liquid/liquid assembled thin films of MoS_2 nanosheets as the channel material. The resulting devices display good mobility and on/off ratio with minimal surface treatment, exhibiting equivalent performance to previously reported mechanically exfoliated single-crystal MoS_2 transistors with matching device layouts. These properties compare well with those of solution-processed and CVD-grown MoS_2-based transistors reported in the literature while requiring minimal postprocessing steps. We attribute this improved performance to the ultrathin and flat nature of the film and the increased proportion of edge-to-edge contacts between flakes achieved by this liquid/liquid assembly method.

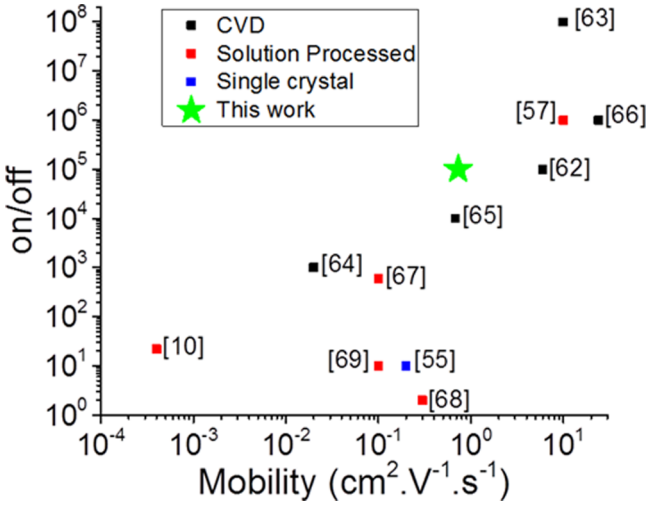

Figure 6. Electrical performance of the FET produced in this work (green star) compared with literature data for FETs manufactured using single mechanically cleaved few-layer MoS_2 crystal (blue symbols) CVD-grown MoS_2 thin films (black symbols) and solution-processed thin films (red symbols). Data source indicated adjacent to each plotted point. Full data is in the Supporting Information, Table S1.[10,55,57,62−69]

The process is scalable, with the potential to be adapted to roll-to-roll processing and could be applied to other 2D, 1D, and 0D materials. Furthermore, ultrapure and degassed solvents can be used as the upper and lower phases to allow the technique to be used in the assembly of air-sensitive materials such as BP and InSe, and we are currently exploring these possibilities.

https://dx.doi.org/10.1021/acsami.0c03794
ACS Appl. Mater. Interfaces 2020, 12, 25125−25134

MATERIALS AND METHODS

Exfoliation of MoS_2. Thin flakes of MoS_2 were prepared using the electrochemical method previously described by Lin et al.[57] This uses the intercalation of bulky tetraheptylammonium (THA) ions to expand the layers within a molybdenite crystal. Since fewer ions are inserted in comparison to the smaller ions used in some intercalation experiments (e.g., Li^+), the 2H semiconducting phase of MoS_2 is retained.[70] A molybdenite crystal (SPI supplies, West Chester, PA 19381-0656) was used as the cathode, and a graphite strip (Gee Graphite Ltd., Dewsbury, U.K.) as the anode in a two-electrode electrochemical cell. A solution of tetraheptylammonium bromide (THAB) (Sigma, Dorset, U.K., ≥99.0%) in acetonitrile (Sigma, ≥99.5%) (40 mL, 12.5 mg mL^{-1}) acts as the electrolyte. The $[THA^+]$ ions were inserted into the layers of the molybdenite crystal under a potential difference of −10 V for 1 h. The expanded molybdenite crystal was washed thoroughly with ethanol (Sigma, 96%) before being sonicated in a 200 mg mL^{-1} poly(vinylpyrrolidone) (PVP) (Sigma, 30 000 mw) in dimethylformamide (DMF) (Sigma, 99.8%) solution using an ultrasonic bath (P120H, Elmasonic, Singen, Germany) 100 W, for 30 min at 30% power. The material formed a bright green dispersion after the sonication step.

The exfoliated dispersion was separated according to nanoflake size using cascade centrifugation (1−16, Sigma, Osterode am Harz, Germany). Centrifugation speed of 5900 and 13 200 relative centrifugal force (RCF) for 20 min per step were used to separate nanoflakes of different sizes. After each sedimentation speed, the solid sedimented material was redispersed in isopropyl alcohol (IPA) (>99.5%, Sigma) and then washed three times by pelleting in a centrifuge and redispersion in IPA. The material pelleted at 13 200 RCF was used in film assembly and the manufacture of the devices herein. XRD patterns for the MoS_2 dispersion, as exfoliated and after size selection, are available in the Supporting Information (Figure S5).

Liquid/Liquid Interfacial Thin-Film Assembly. Thin films were assembled at the interface between an upper phase of hexane (Sigma, ≥99%), density 655 kg m^{-3}, and a lower phase of deionized water, density 995 kg m^{-3}, in a 50 mL glass beaker. The tip of a glass Pasteur pipette containing around 0.4 mL of the dispersion of nanoflakes in IPA (Sigma), density 786 kg m^{-3}, was inserted into the hexane layer. As the dispersion has a higher density than hexane, the IPA dispersion slowly falls from the tip of the pipette to merge with the hexane/water interface. The hexane exchanges with IPA in the closed system until all of the material from the dispersion assembles into a film parallel to the interface; this takes approximately 2 min, depending on the size of the interface and the 2D material used. All of the IPA is eventually exchanged for hexane, completing the transfer of the nanoflake material to the interface. The progress of film deposition can easily be seen by the naked eye (Supporting Information, Video S1); furthermore, the addition of the dispersion can be arrested when the interface is seen to be filled with a monolayer of nanoflakes. The resulting film of the 2D material can then be coated onto a variety of substrates by placing a substrate aligned parallel to and then lifting it through the interface, analogous to the Langmuir−Schaeffer coating method (Figure 2b).[41] The substrate was lifted using a dip coater (Dip Coater, Ossilla, Sheffield, U.K.).

Spin-Coating Thin-Film Assembly. Two widely used methods of solution-processed film deposition are spin coating and spray coating. These methods were used as comparison/controls with the liquid/liquid interface assembly method. Spin coating uses a spinning chuck, which holds the substrate to be coated and spreads the coating liquid over the substrate using centrifugal force. In a typical thin-film assembly, MoS_2 dispersion was spin-coated (Ossilla) onto 645 mm^2 (1 in^2) Si/SiO_2, 90 nm wafer coupons 3−10 times at 2000 RPM for 20 s. The number of deposition cycles was chosen to specify the areal density of flakes on the surface. With spin coating, only a fraction of each dispersion is coated per cycle; hence, coatings were selected for comparison with those produced by liquid/liquid assembly by choosing those with similar mean coverage.

Spray-Coating Thin-Film Assembly. Spray coating was carried out using an airbrush tool (Infinity, Harder and Steenbeck, Norderstedt, Germany) to deposit MoS_2 dispersions onto the substrate. Typically, the MoS_2 dispersion (0.5 mL) was added to the airbrush reservoir and the airbrush was held at a distance of 11 cm from the substrate. The substrate was heated to a temperature of 90 °C, and the dispersion was sprayed onto the surface in 1 s bursts. The number of bursts was chosen to specify the areal density of flakes on the surface. As with spin coating, there are losses of suspension that do not deposit per cycle (overspray) and coatings for comparison purposes were selected by inspection after deposition.

Flake and Film Characterization. Flake thicknesses were measured using an atomic force microscope (AFM) (Dimension FastScan, Bruker, Billerica, MA). AFM scans were performed using Antimony (n)-doped Si TESPA-V2 probe tips (Bruker). Scanning electron microscopy (SEM) images of the liquid/liquid assembled films on substrates were obtained using an Ultra 55 FEG SEM (Zeiss, Oberkochen, Germany). XRD patterns were obtained using a Rigaku SmartLab X-ray diffractometer (Rigaku, Tokyo, Japan). UV−vis spectroscopy was performed using a Lambda 25 spectrometer (Perkin Elmer, Waltham, MA).

Lateral flake areas were measured using manipulation of an SEM image of nanoflakes with the Fiji software.[71] First, the SEM image was thresholded to maximize the contrast of the flake area against the substrate area. Next, the "analyze particles" function was used to count the area of each of the particles in the image (n = 714) and calculate the mean lateral flake area. A histogram of the flake areas generated by this analysis is given in the Supporting Information, Figure S1b.

The AFM images were processed and manipulated using the Gwyddion software.[72] Scans were leveled using average plane fitting. The individual scan lines were then flattened using a median of averages. Any large scars caused by impurities in the film were cropped from the final scan area. The substrate plane was then flattened using the three-point method by manually selecting three locations where the substrate was visible (in thick films, where the uncovered substrate cannot be clearly seen, the film can be scratched away using polyether ether ketone (PEEK) tipped tweezers to select three points to level the plane of the substrate). The z-height value (relative to the leveled substrate) for each pixel in the scan area was used to generate the histograms in Figure 4.

Poisson distributions were fitted to AFM histograms (Figure 4d−f) using the Origin software (Origin(Pro), Version 2015, OriginLab Corporation, Northampton, MA). The averaged data points with standard deviation were fitted using the Levenberg−Marquardt fitting algorithm and statistical weighting.

Three-Phase Contact Angle Measurement. The three-phase contact angle at the water, hexane, and MoS_2 contact line was found using the sessile drop method. A droplet of deionized water was placed on the surface of a MoS_2 crystal (SPI supplies), which was submerged in hexane (99%, Sigma). The three-phase contact angle was recorded using a drop shape analyzer (DSA100, Kruss, Hamburg, Germany).

Device Manufacture and Testing. To fabricate transistors, n-doped silicon substrates, OFET test chip, and 230 nm SiO_2 (IPMS Fraunhofer, Dresden, Germany), with prefabricated interdigitated electrodes (ITO 10 nm, Au 30 nm), were first washed in acetone, water, and IPA with sonication for 10 min with each solvent. The substrates were then coated with the MoS_2 thin film using our liquid/liquid assembly method. The film was heated in a tube furnace (MTF, Carbolite, Hope, U.K.) in an Ar atmosphere for 2 h at 200 °C. The devices were tested immediately after removal from the furnace with no surface treatment. Some devices were also soaked in deionized water overnight after the heat treatment to remove any retained (THAB) from the exfoliation step. The n-doped silicon acts as a back gate, while the thin film of MoS_2 nanosheets acts as the channel. The interdigitated electrodes are the source and drain for the back gate/back contact (BG/BC) device (Figure 5a).

Device testing was performed using a source meter (2400 series, Keithley, Solon, OH) and a probe station (PE4, Everbeing, Hsinchu City, Taiwan).

https://dx.doi.org/10.1021/acsami.0c03794
ACS Appl. Mater. Interfaces 2020, 12, 25125−25134

■ ASSOCIATED CONTENT

Supporting Information

The Supporting Information is available free of charge at https://pubs.acs.org/doi/10.1021/acsami.0c03794.

Bond number calculation for MoS_2 particles at the interface, demonstrating that capillary forces dominate gravitational forces; thickness and lateral size data for the MoS_2 dispersion; high-magnification SEM image of the MoS_2 liquid/liquid assembled thin film; transfer curves of three repeat FET devices; drop watcher image of the three-phase contact angle among MoS_2, water, and hexane interfaces; XRD patterns for liquid/liquid interface assembled thin films of MoS_2 flakes; table providing literature values used to produce main text (Figure 6) (PDF)

Liquid/liquid assembly method (Video) (MP4)

■ AUTHOR INFORMATION

Corresponding Author

Brian Derby − *Department of Materials, University of Manchester, Manchester M13 9PL, U.K.;* orcid.org/0000-0001-5753-0166; Email: brian.derby@manchester.ac.uk

Authors

Joseph Neilson − *Department of Materials, University of Manchester, Manchester M13 9PL, U.K.;* orcid.org/0000-0002-2472-4869

Michael P. Avery − *Department of Materials, University of Manchester, Manchester M13 9PL, U.K.;* orcid.org/0000-0002-2154-1354

Complete contact information is available at: https://pubs.acs.org/10.1021/acsami.0c03794

Notes

The authors declare no competing financial interest.

■ ACKNOWLEDGMENTS

We acknowledge the support of EPSRC through grant EP/N010345/1 and for studentship support for J.N. (ref 1811873). We also acknowledge the Henry Royce Institute for Advanced Materials, for provision of facilities through EPSRC grants: EP/R00661X/1, EP/S019367/1, EP/P025021/1, and EP/P025498/. We wish to thank Maddison Coke for assistance in acquiring and interpreting the XRD image data, William Sampson for helpful discussions and advice on statistical analysis, and David Lewis for his helpful discussions and assistance.

■ REFERENCES

(1) Novoselov, K. S.; Geim, A. K.; Morozov, S. V.; Jiang, D.; Zhang, Y.; Dubonos, S. V.; Grigorieva, I. V.; Firsov, A. A. Electric Field Effect in Atomically Thin Carbon Films. *Science* **2004**, *306*, 666−669.

(2) Roy, T.; Tosun, M.; Kang, J. S.; Sachid, A. B.; Desai, S. B.; Hettick, M.; Hu, C. C.; Javey, A. Field-Effect Transistors Built from All Two-Dimensional Material Components. *ACS Nano* **2014**, *8*, 6259−6264.

(3) Cui, X.; Lee, G.-H.; Kim, Y. D.; Arefe, G.; Huang, P. Y.; Lee, C.-H.; Chenet, D. A.; Zhang, X.; Wang, L.; Ye, F.; Pizzocchero, F.; Jessen, B. S.; Watanabe, K.; Taniguchi, T.; Muller, D. A.; Low, T.; Kim, P.; Hone, J. Multi-Terminal Transport Measurements of MoS_2 Using a van Der Waals Heterostructure Device Platform. *Nat. Nanotechnol.* **2015**, *10*, 534−540.

(4) Huo, N.; Konstantatos, G. Ultrasensitive All-2D MoS_2 Phototransistors Enabled by an out-of-Plane MoS_2 PN Homojunction. *Nat. Commun.* **2017**, *8*, No. 572.

(5) Kwon, H.; Garg, S.; Park, J. H.; Jeong, Y.; Yu, S.; Kim, S. M.; Kung, P.; Im, S. Monolayer MoS_2 Field-Effect Transistors Patterned by Photolithography for Active Matrix Pixels in Organic Light-Emitting Diodes. *npj 2D Mater. Appl.* **2019**, *3*, No. 9.

(6) Lee, Y. H.; Zhang, X. Q.; Zhang, W.; Chang, M. T.; Lin, C. T.; Chang, K. D.; Yu, Y. C.; Wang, J. T. W.; Chang, C. S.; Li, L. J.; Lin, T. W. Synthesis of Large-Area MoS_2 Atomic Layers with Chemical Vapor Deposition. *Adv. Mater.* **2012**, *24*, 2320−2325.

(7) Bässler, H.; Köhler, A. Charge Carrier Mobility in Amorphous Organic Semiconductors. In *Organic Light-Emitting Diodes (OLEDs)*; Buckley, A., Ed.; Elsevier, 2013; pp 192−234.

(8) Nicolosi, V.; Chhowalla, M.; Kanatzidis, M. G.; Strano, M. S.; Coleman, J. N. Liquid Exfoliation of Layered. *Mater. Sci.* **2013**, *340*, No. 1226419.

(9) Zhu, J.; Kang, J.; Kang, J.; Jariwala, D.; Wood, J. D.; Seo, J. W. T.; Chen, K. S.; Marks, T. J.; Hersam, M. C. Solution-Processed Dielectrics Based on Thickness-Sorted Two-Dimensional Hexagonal Boron Nitride Nanosheets. *Nano Lett.* **2015**, *15*, 7029−7036.

(10) Zeng, X.; Hirwa, H.; Metel, S.; Nicolosi, V.; Wagner, V. Solution Processed Thin Film Transistor from Liquid Phase Exfoliated MoS_2 Flakes. *Solid State Electron.* **2018**, *141*, 58−64.

(11) Becerril, H. A.; Mao, J.; Liu, Z.; Stoltenberg, R. M.; Bao, Z.; Chen, Y. Evaluation of Solution-Processed Reduced Graphene Oxide Films as as Transparent Conductors. *ACS Nano* **2008**, *2*, 463−470.

(12) Cote, L. J.; Kim, F.; Huang, J. Langmuir-Blodgett Assembly of Graphite Oxide Single Layers. *J. Am. Chem. Soc.* **2009**, *131*, 1043−1049.

(13) Zhang, Y.; Xu, L.; Walker, W. R.; Tittle, C. M.; Backhouse, C. J.; Pope, M. A. Langmuir Films and Uniform, Large Area, Transparent Coatings of Chemically Exfoliated MoS_2 Single Layers. *J. Mater. Chem. C* **2017**, *5*, 11275−11287.

(14) Ariga, K.; Yamauchi, Y.; Mori, T.; Hill, J. P. 25th Anniversary Article: What Can Be Done with the Langmuir-Blodgett Method? Recent Developments and Its Critical Role in Materials Science. *Adv. Mater.* **2013**, *25*, 6477−6512.

(15) Booth, S. G.; Dryfe, R. A. W. Assembly of Nanoscale Objects at the Liquid/Liquid Interface. *J. Phys. Chem. C* **2015**, *119*, 23295−23309.

(16) Biswas, S.; Drzal, L. T. A Novel Approach to Create a Highly Ordered Monolayer Film of Graphene Nanosheets at the Liquid−Liquid Interface. *Nano Lett.* **2009**, *9*, 167−172.

(17) Jia, B.; Wang, Q.; Zhang, W.; Lin, B.; Yuan, N.; Ding, J.; Ren, Y.; Chu, F. A New Oil/Water Interfacial Assembly of Sulphonated Graphene into Ultrathin Films. *RSC Adv.* **2014**, *4*, 34566−34571.

(18) Yu, X.; Prévot, M. S.; Guijarro, N.; Sivula, K. Self-Assembled 2D WSe_2 Thin Films for Photoelectrochemical Hydrogen Production. *Nat. Commun.* **2015**, *6*, No. 7596.

(19) Hu, L.; Ma, R.; Ozawa, T. C.; Geng, F.; Iyi, N.; Sasaki, T. Oriented Films of Layered Rare-Earth Hydroxide Crystallites Self-Assembled at the Hexane/Water Interface. *Chem. Commun.* **2008**, *402*, 4897−4899.

(20) Woltornist, S. J.; Oyer, A. J.; Carrillo, J. M. Y.; Dobrynin, A. V.; Adamson, D. H. Conductive Thin Films of Pristine Graphene by Solvent Interface Trapping. *ACS Nano* **2013**, *7*, 7062−7066.

(21) Clark, R. M.; Berean, K. J.; Carey, B. J.; Pillai, N.; Daeneke, T.; Cole, I. S.; Latham, K.; Kalantar-zadeh, K. Patterned Films from Exfoliated Two-Dimensional Transition Metal Dichalcogenides Assembled at a Liquid−Liquid Interface. *J. Mater. Chem. C* **2017**, *5*, 6937−6944.

(22) Nie, H. L.; Dou, X.; Tang, Z.; Jang, H. D.; Huang, J. High-Yield Spreading of Water-Miscible Solvents on Water for Langmuir-Blodgett Assembly. *J. Am. Chem. Soc.* **2015**, *137*, 10683−10688.

(23) Xiao, P.; Gu, J.; Wan, C.; Wang, S.; He, J.; Zhang, J.; Huang, Y.; Kuo, S. W.; Chen, T. Ultrafast Formation of Free-Standing 2D Carbon Nanotube Thin Films through Capillary Force Driving

Compression on an Air/Water Interface. *Chem. Mater.* **2016**, *28*, 7125−7133.
(24) Sangwan, V. K.; Hersam, M. C. Electronic Transport in Two-Dimensional Materials. *Annu. Rev. Phys. Chem.* **2018**, *69*, 299−325.
(25) Wang, L.; Meric, I.; Huang, P. Y.; Gao, Q.; Gao, Y.; Tran, H.; Taniguchi, T.; Watanabe, K.; Campos, L. M.; Muller, D. A.; Guo, J.; Kim, P.; Hone, J.; Shepard, K. L.; Dean, C. R. One-Dimensional Electrical Contact to a Two-Dimensional Material. *Science* **2013**, *342*, 614−617.
(26) Allain, A.; Kang, J.; Banerjee, K.; Kis, A. Electrical Contacts to Two-Dimensional Semiconductors. *Nat. Mater.* **2015**, *14*, 1195−1205.
(27) Xu, Y.; Cheng, C.; Du, S.; Yang, J.; Yu, B.; Luo, J.; Yin, W.; Li, E.; Dong, S.; Ye, P.; Duang, X. Contacts between Two- and Three-Dimensional Materials: Ohmic, Schottky, and p−n Heterojunctions. *ACS Nano* **2016**, *10*, 4895−4919.
(28) Gan, S.; Zhong, L.; Wu, T.; Han, D.; Zhang, J.; Ulstrup, J.; Chi, Q.; Niu, L. Spontaneous and Fast Growth of Large-Area Graphene Nanofilms Facilitated by Oil/Water Interfaces. *Adv. Mater.* **2012**, *24*, 3958−3964.
(29) Zeppieri, S.; Rodríguez, J.; López De Ramos, A. L. Interfacial Tension of Alkane + Water Systems. *J. Chem. Eng. Data* **2001**, *46*, 1086−1088.
(30) Shen, J.; He, Y.; Wu, J.; Gao, C.; Keyshar, K.; Zhang, X.; Yang, Y.; Ye, M.; Vajtai, R.; Lou, J.; Ajayan, P. M. Liquid Phase Exfoliation of Two-Dimensional Materials by Directly Probing and Matching Surface Tension Components. *Nano Lett.* **2015**, *15*, 5449−5454.
(31) Wilson, J. A.; Yoffe, A. D. The Transition Metal Dichalcogenides Discussion and Interpretation of the Observed Optical, Electrical and Structural Properties. *Adv. Phys.* **1969**, *18*, 193−335.
(32) Qiu, D. Y.; da Jornada, F. H.; Louie, S. G. Optical Spectrum of MoS_2: Many-body Effects and Diversity of Exciton States. *Phys. Rev. Lett.* **2013**, *111*, No. 216805.
(33) Mak, K. F.; Lee, C.; Hone, J.; Shan, J.; Heinz, T. F. Atomically Thin MoS_2: A New Direct-Gap Semiconductor. *Phys. Rev. Lett.* **2010**, *105*, No. 136805.
(34) Tauc, J.; Grigorovici, R.; Vancu, A. Optical Properties and Electronic Structure of Amorphous Germanium. *Phys. Status Solidi* **1966**, *15*, 627−637.
(35) Pieranski, P. Two-Dimensional Interfacial Colloidal Crystals. *Phys. Rev. Lett.* **1980**, *45*, 569−572.
(36) Binks, B. P.; Horozov, T. S. Colloidal Particles at Liquid Interfaces: An Introduction. In *Colloidal Particles at Liquid Interfaces*; Binks, B. P.; Horozov, T. S., Eds.; Cambridge University Press: Cambridge, 2006; pp 1−74.
(37) Fei, W.; Gu, Y.; Bishop, K. J. M. Active Colloidal Particles at Fluid-Fluid Interfaces. *Curr. Opin. Colloid Interface Sci.* **2017**, *32*, 57−68.
(38) Binks, B. P. Particles as Surfactants—Similarities and Differences. *Curr. Opin. Colloid Interface Sci.* **2002**, *7*, 21−41.
(39) Chevalier, Y.; Bolzinger, M. A. Emulsions Stabilized with Solid Nanoparticles: Pickering Emulsions. *Colloids Surf., A* **2013**, *439*, 23−34.
(40) Paul, G. W.; Marc de Chazal, L. E. Interfacial Tensions in Ternary Liquid-Liquid Systems. *J. Chem. Eng. Data* **1967**, *12*, 105−107.
(41) Langmuir, I.; Schaefer, V. J. Activities of Urease and Pepsin Monolayers. *J. Am. Chem. Soc.* **1938**, *60*, 1351−1360.
(42) Okahata, Y.; Ariga, K.; Tanaka, K. Evaluation of a Horizontal Lifting Method of Langmuir-Blodgett Films Using a Quartz-Crystal Microbalance. *Thin Solid Films* **1992**, *210−211*, 702−706.
(43) Xu, X.; Rice, S. A. Maximally Random Jamming of One-Component and Binary Hard-Disk Fluids in Two Dimensions. *Phys. Rev. E* **2011**, *83*, No. 021120.
(44) Donev, A.; Torquato, S.; Stillinger, F. H.; Connelly, R. Jamming in Hard Sphere and Disk Packings. *J. Appl. Phys.* **2004**, *95*, 989−999.
(45) Delaney, G.; Weaire, D.; Hutzler, S.; Murphy, S. Random Packing of Elliptical Disks. *Philos. Mag. Lett.* **2005**, *85*, 89−96.
(46) Quickenden, T. I.; Tan, G. K. Random Packing in Two Dimensions and the Structure of Monolayers. *J. Colloid Interface Sci.* **1974**, *48*, 382−393.
(47) Okubo, T.; Odagaki, T. Random Packing of Binary Hard Discs. *J. Phys. Condens. Matter* **2004**, *16*, 6651−6659.
(48) Hinrichsen, E. L.; Feder, J.; Jøssang, T. Random Packing of Disks in Two Dimensions. *Phys. Rev. A* **1990**, *41*, 4199−4209.
(49) Ainsworth, C. A.; Derby, B.; Sampson, W. W. Interdependence of Resistance and Optical Transmission in Conductive Nanowire Networks. *Adv. Theory Simul.* **2018**, *1*, No. 1700011.
(50) Sampson, W. W. *Modelling Stochastic Fibrous Materials with Mathematica*; Springer London: London, 2009; pp 105−157.
(51) Bowden, N. Self-Assembly of Mesoscale Objects into Ordered Two-Dimensional Arrays. *Science* **1997**, *276*, 233−235.
(52) Kralchevsky, P. A.; Nagayama, K. Lateral Capillary Forces between Partially Immersed Bodies. In *Studies in Interface Science*; Kralchevsky, P. A.; Nagayama, K., Eds.; 2001; pp 287−350.
(53) Ramakrishna Matte, H. S. S.; Gomathi, A.; Manna, A. K.; Late, D. J.; Datta, R.; Pati, S. K.; Rao, C. N. R. MoS_2 and WS_2 Analogues of Graphene. *Angew. Chem., Int. Ed.* **2010**, *49*, 4059−4062.
(54) Rao, C. N. R.; Nag, A. Inorganic Analogues of Graphene. *Eur. J. Inorg. Chem.* **2010**, *27*, 4244−4250.
(55) Novoselov, K. S.; Jiang, D.; Schedin, F.; Booth, T. J.; Khotkevich, V. V.; Morozov, S. V.; Geim, A. K. Two-dimensional atomic crystals. *Proc. Natl. Acad. Sci. U.S.A.* **2005**, *102*, 10451−10453.
(56) Radisavljevic, B.; Radenovic, A.; Brivio, J.; Giacometti, V.; Kis, A. Single-layer MoS_2 transistors. *Nat. Nanotechnol.* **2011**, *6*, 147−150.
(57) Lin, Z.; Liu, Y.; Halim, U.; Ding, M.; Liu, Y.; Wang, Y.; Jia, C.; Chen, P.; Duan, X.; Wang, C.; Song, F.; Li, M.; Wan, C.; Huang, Y.; Duan, X. Solution-Processable 2D Semiconductors for High-Performance Large-Area Electronics. *Nature* **2018**, *562*, 254−258.
(58) Jena, D.; Konar, A. Enhancement of Carrier Mobility in Semiconductor Nanostructures by Dielectric Engineering. *Phys. Rev. Lett.* **2007**, *98*, No. 136805.
(59) Alharbi, A.; Zahl, P.; Shahrjerdi, D. Material and Device Properties of Superacid Treated Monolayer Molybdenum Disulfide. *Appl. Phys. Lett.* **2017**, *110*, No. 033503.
(60) Qiu, H.; Pan, L. J.; Yao, Z.; Li, J.; Shi, Y.; Wang, X. Electrical characterization of back-gated bilayer MoS_2 field-effect transistors and the effect of ambient on their performances. *Appl. Phys. Lett.* **2012**, *100*, No. 123104.
(61) Tosun, M.; Fu, D.; Desai, S. B.; Ko, C.; Kang, J. S.; Lien, D.-H.; Najmzadeh, M.; Tongay, S.; Wu, J.; Javey, A. MoS2 Heterojunctions by Thickness Modulation. *Sci. Rep.* **2015**, *5*, No. 10990.
(62) Amani, M.; Chin, M. L.; Birdwell, A. G.; O'Regan, T. P.; Najmaei, S.; Liu, Z.; Ajayan, P. M.; Lou, J.; Dubey, M. Electrical Performance of Monolayer MoS_2 Field-Effect Transistors Prepared by Chemical Vapor Deposition. *Appl. Phys. Lett.* **2013**, *102*, No. 193107.
(63) Wu, W.; De, D.; Chang, S.-C.; Wang, Y.; Peng, H.; Bao, J.; Pei, S.-S. High Mobility and High on/off Ratio Field-Effect Transistors Based on Chemical Vapor Deposited Single-Crystal MoS_2 Grains. *Appl. Phys. Lett.* **2013**, *102*, No. 142106.
(64) Lee, Y.-H.; Zhang, X.-Q.; Zhang, W.; Chang, M.-T.; Lin, C.-T.; Chang, K.-D.; Yu, Y.-C.; Wang, J. T.-W.; Chang, C.-S.; Li, L.-J.; Lin, T.-W. Synthesis of Large-Area MoS_2 Atomic Layers with Chemical Vapor Deposition. *Adv. Mater.* **2012**, *24*, 2320−2325.
(65) Wen, M.; Xu, J. P.; Liu, L.; Zhao, X.; Lai, P. T.; Tang, W. M. In Fabrication and Electrical Performance of CVD-Grown MoS_2 Transistor. *2017 IEEE International Conference on Electron Devices Solid-State Circuits*, 2017; pp 1−3.
(66) Kappera, R.; Voiry, D.; Yalcin, S. E.; Jen, W.; Acerce, M.; Torrel, S.; Branch, B.; Lei, S.; Chen, W.; Najmaei, S.; Lou, J.; Ajayan, P. M.; Gupta, G.; Mohite, A. D.; Chhowalla, M. Metallic 1T Phase Source/Drain Electrodes for Field Effect Transistors from Chemical Vapor Deposited MoS_2. *APL Mater.* **2014**, *2*, No. 092516.
(67) Kelly, A. G.; Hallam, T.; Backes, C.; Harvey, A.; Esmaeily, A. S.; Godwin, I.; Coelho, J.; Nicolosi, V.; Lauth, J.; Kulkarni, A.; Kinge, S.; Siebbeles, L. D. A.; Duesberg, G. S.; Coleman, J. N. All-Printed Thin-

https://dx.doi.org/10.1021/acsami.0c03794
ACS Appl. Mater. Interfaces 2020, 12, 25125−25134

Film Transistors from Networks of Liquid-Exfoliated Nanosheets. *Science* **2017**, *356*, 69−73.
(68) He, Q.; Zeng, Z.; Yin, Z.; Li, H.; Wu, S.; Huang, X.; Zhang, H. Fabrication of Flexible MoS_2 Thin-Film Transistor Arrays for Practical Gas-Sensing Applications. *Small* **2012**, *8*, 2994−2999.
(69) Li, J.; Naiini, M. M.; Vaziri, S.; Lemme, M. C.; Östling, M. Inkjet Printing of MoS_2. *Adv. Funct. Mater.* **2014**, *24*, 6524−6531.
(70) Joensen, P.; Frindt, R. F.; Morrison, S. R. Single-Layer MoS_2. *Mater. Res. Bull.* **1986**, *21*, 457−461.
(71) Schindelin, J.; Arganda-Carreras, I.; Frise, E.; Kaynig, V.; Longair, M.; Pietzsch, T.; Preibisch, S.; Rueden, C.; Saalfeld, S.; Schmid, B.; Tinevez, J. Y.; White, D. J.; Hartenstein, V.; Eliceiri, K.; Tomancak, P.; Cardona, A. Fiji: An Open-Source Platform for Biological-Image Analysis. *Nat. Methods* **2012**, *9*, 676−682.
(72) Nečas, D.; Klapetek, P. Gwyddion: An Open-Source Software for SPM Data Analysis. *Cent. Eur. J. Phys.* **2012**, *10*, 181−188.

https://dx.doi.org/10.1021/acsami.0c03794
ACS Appl. Mater. Interfaces 2020, 12, 25125−25134